Nitrous oxide variability at sub-kilometre resolution in the Atlantic sector of the Southern Ocean

Imke Grefe[1,3], Sophie Fielding[2], Karen J. Heywood[1] and Jan Kaiser[1]

[1] Centre for Ocean and Atmospheric Sciences, University of East Anglia, Norwich, United Kingdom
[2] British Antarctic Survey, Cambridge, United Kingdom
[3] Current affiliation: Lancaster Environment Centre, Lancaster University, Lancaster, United Kingdom

ABSTRACT

The Southern Ocean is an important region for global nitrous oxide (N_2O) cycling. The contribution of different source and sink mechanisms is, however, not very well constrained due to a scarcity of seawater data from the area. Here we present high-resolution surface N_2O measurements from the Atlantic sector of the Southern Ocean, taking advantage of a relatively new underway setup allowing for collection of data during transit across mesoscale features such as frontal systems and eddies. Covering a range of different environments and biogeochemical settings, N_2O saturations and sea-to-air fluxes were highly variable: Saturations ranged from 96.5% at the sea ice edge in the Weddell Sea to 126.1% across the Polar Frontal Zone during transit to South Georgia. Negative sea-to-air fluxes (N_2O uptake) of up to -1.3 μmol m^{-2} d^{-1} were observed in the Subantarctic Zone and highest positive fluxes (N_2O emission) of 14.5 μmol m^{-2} d^{-1} in Stromness Bay, coastal South Georgia. Although N_2O saturations were high in areas of high productivity, no correlation between saturations and chlorophyll a (as a proxy for productivity) was observed. Nevertheless, there is a clear effect of islands and shallow bathymetry on N_2O production as inferred from supersaturations.

INTRODUCTION

Nitrous oxide (N_2O) is a strong greenhouse gas and currently the third largest contributor to radiative forcing after carbon dioxide (CO_2) and methane (CH_4) (*Hartmann et al., 2013*). Furthermore, N_2O is an important source for stratospheric NO_x, which is involved in catalytic ozone depletion (*Crutzen, 1970*; *Ravishankara, Daniel & Portmann, 2009*). The oceans, including coastal zones, estuaries and rivers, are estimated to contribute approximately 25% to global N_2O emissions (*Ciais et al., 2013*). The Southern Ocean alone is estimated to account for 5% of global emissions (0.9 Tg a^{-1} N (nitrogen equivalents), (*Nevison et al., 2005*)). However, measurements of oceanic N_2O concentrations in this region are scarce and these emission estimates are based on atmospheric measurements at Cape Grim and a few seawater measurements in the Southern Ocean from 1977–1993 (*Nevison, Weiss & Erickson, 1995*; *Nevison et al., 2005* and references therein).

In the ocean N_2O is produced as a byproduct during nitrification and an intermediate during nitrifier-denitrification in oxygenated waters, and as an intermediate during denitrification in anoxic waters. Nitrification is a two-step process during which ammonia oxidation is followed by nitrite oxidation. The first step is carried out by ammonia oxidising bacteria (AOB) and archaea (AOA). N_2O is a by-product of this step that can be produced during hydroxylamine or nitric oxide oxidation (*Ward, 2008* and references therein). Only recently both steps of nitrification, ammonia oxidation and nitrite oxidation, have been observed in one organism (*Daims et al., 2015*; *Van Kessel et al., 2015*).

Nitrifier-denitrification is the process of ammonia oxidation to nitrite, followed by nitrite reduction via NO and N_2O to N_2 (*Wrage et al., 2001*).

Denitrification takes place under anoxic conditions where NO_3^- acts as an electron acceptor in the absence of oxygen ((*Devol, 2008*) and references therein). NO_3^- is reduced to NO_2^-, NO and N_2O. At the core of oxygen minimum zones, N_2O is further reduced to N_2 (*Bange, 2008* and references therein).

The solubility of N_2O in seawater has been described by *Weiss & Price (1980)*. N_2O is a soluble gas, similar to CO_2. Due to its high solubility physical processes such as bubble effects do not have a strong effect on surface N_2O saturations. Warming and cooling of surface waters also has only a small effect (4% per degree centigrade). Due to the non-linearity of saturation curves for water mass mixing, diapycnal mixing, upwelling and entrainment of deeper water masses into the surface only has an impact on N_2O saturations if there is a large concentration gradient. Examples for high N_2O surface saturations due to these processes are rising isopycnals at the Southern Antarctic Circumpolar Current Front (SACCF, see below, *Chen et al., 2014* and this work) and upwelling along the California coast (*Lueker et al., 2003*).

The Scotia Sea in the Atlantic sector of the Southern Ocean is confined by the Scotia Ridge to the north, east and south and the Drake Passage to the west (*Atkinson et al., 2001*). South Georgia is part of the North Scotia Ridge in the path of the Antarctic Circumpolar Current (ACC) and within the Antarctic Zone (AAZ) south of the Polar Front (PF).

The ACC is driven by strong, westerly winds between approximately 45–55°S (*Trenberth, Large & Olson, 1990*) and connects the Atlantic, Pacific and Indian Ocean. Isopycnals rise step-wise towards the south, characterising the ACC fronts and their resulting strong surface currents (*Orsi, Whitworth & Nowlin, 1995* and references within): the Subantarctic Front (SAF), Polar Front (PF) and the Southern ACC Front (SACCF), accounting for most of the ACC transport. The SAF is characterised by the rapid subduction of the salinity minimum of Antarctic Intermediate Water (AAIW) to the north (*Whitworth & Nowlin, 1987*). Subduction of the temperature minimum of the AASW marks the position of the PF (*Gordon, 1967*). The SACCF is then characterised by a subsurface horizontal temperature gradient as Upper Circumpolar Deep Water (UCDW) shoals to the south. The Southern Boundary of the ACC (SB) can be identified by a loss of UCDW properties (temperature, salinity, oxygen minimum) to the south. To the north of the SB the UCDW isopycnal shoals and UCDW can be entrained into the Surface Mixed Layer (SML) (*Orsi, Whitworth & Nowlin, 1995*). The Weddell-Scotia Confluence separates the ACC from the waters of the Weddell Gyre (*Gordon, 1967*) and is a regional feature of the Scotia Sea.

Grefe et al. (2018), *PeerJ*, DOI 10.7717/peerj.5100

2/28

Around South Georgia, the path of the ACC is strongly influenced by the bathymetry (*Atkinson et al., 2001* and references therein): The South Georgia Ridge to the west of the island deflects the ACC to the north, resulting in strong large- and mesoscale variability. Additionally, the wide shelf seems to influence temperature and salinity in the waters around the island. It was observed that in summer the water is slightly warmer and fresher than in the surrounding ocean, possibly due to solar heating of the shallow water column and local runoff, respectively (*Priddle, Heywood & Theriot, 1986*; *Brandon et al., 2000*).

Waters around South Georgia are characterised by high abundances of phytoplankton, zooplankton and vertebrate predators (*Atkinson et al., 2001*), whereas most other areas of the Southern Ocean are dominated by High Nutrient Low Chlorophyll (HNLC) conditions (*Martin, 1990*). A relatively stable water column and benthic iron input support productivity in the vicinity of the island (*Holeton et al., 2005*; *Korb et al., 2005*).

To the south of the Scotia Sea and the ACC, the Weddell Sea is characterised by a large gyre, flowing eastwards until 20–30°E, returning westwards along the continental margin and following the eastern coast of the Antarctic Peninsula northwards (*Deacon, 1979*). Seasonal blooms in the Weddell Sea are associated with the Antarctic shelf and the ice edge (*El-Sayed & Taguchi, 1981*; *Kristiansen, Syvertsen & Farbrot, 1992*; *Nelson et al., 1989*; *Smith Jr & Nelson, 1990*). Furthermore, drifting icebergs stimulate productivity by input of terrigenous iron through melt water (*Biddle et al., 2015*; *Smith et al., 2007*).

Generally, the Southern Ocean has the potential for both production and removal of N_2O (*Rees, Owens & Upstill-Goddard, 1997*): Solubility of N_2O increases at lower temperatures, and together with downwelling areas associated with deep-water formation and convergences in the Antarctic frontal zones, wide areas could function as sinks. On the other hand, upwelling of deep and intermediate waters could be a source of biologically produced N_2O to the atmosphere. Artificial iron fertilisation of the Southern Ocean may stimulate biological CO_2 uptake, but could potentially increase N_2O production, offsetting the benefits of CO_2 sequestration in terms of radiative forcing (*Fuhrman & Capone, 1991*; *Jin & Gruber, 2003*). While an iron fertilisation experiment in the Australasian sector of the Southern Ocean showed N_2O accumulation in the pycnocline (*Law & Ling, 2001*), no increase in N_2O concentrations was observed during a similar experiment in the Atlantic subpolar sector (*Walter et al., 2005*).

Here, we present high-resolution measurements of ocean surface N_2O concentrations from the Scotia Sea and Weddell Sea. Using laser off-axis Integrated Cavity Output Spectroscopy (ICOS) (*Arevalo-Martinez et al., 2013*; *Grefe & Kaiser, 2014*) combined with wind-speed gas exchange parameterisations we can resolve small-scale variability in N_2O fluxes and capture the impact of frontal structures and changes in weather conditions on emissions from the Southern Ocean.

METHODS

N_2O concentrations in surface waters were measured during the annual Western Core Box (WCB) krill survey in the Scotia Sea between 28 December 2011 and 16 January 2012 (JR260B) and in the Weddell Sea from 20 January to 2 February 2012 (JR255A/GENTOO
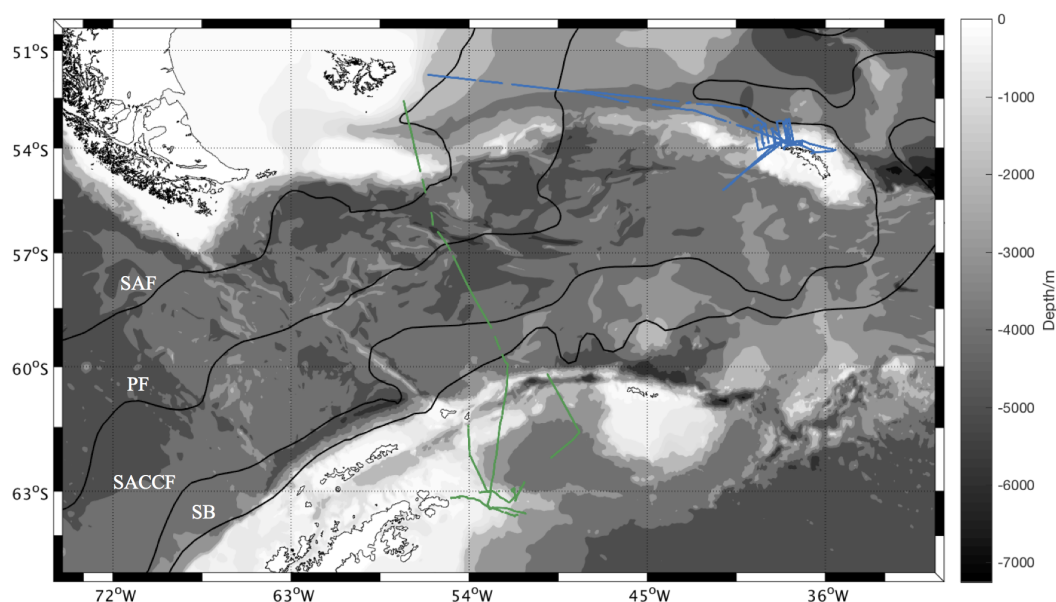
Figure 1 **Overview of sampling area.** Sampling area with bathymetry from the General Bathymetric Chart of the Oceans (GEBCO) one minute grid (*Jakobsson et al., 2008*). Isobaths every 1,000 m between 8,000 m and 1,000 m depth, every 200 m between 1,000 m and 0 m. N_2O measurement positions during JR260B in blue, N_2O measurement positions during JR255A/GENTOO in green. Climatological locations of fronts in black given in *Orsi, Whitworth & Nowlin (1995)*: SAF Sub-Antarctic Front, PF Polar Front, SACCF Southern Antarctic Circumpolar Current Front, SB Southern Boundary of the Antarctic Circumpolar Current.

Full-size ☒ DOI: 10.7717/peerj.5100/fig-1

Gliders: Excellent New Tools for Observing the Ocean) on board RRS *James Clark Ross*. The measurement region for both cruises is shown in Fig. 1.

The setup and performance of the coupled analyser-equilibrator system is described in *Grefe & Kaiser (2014)*. Briefly, a percolating glass bed equilibrator was connected to a N_2O/CO analyser (N_2O/CO-23d, Los Gatos Research Inc.). Artificial air mixtures (21% O_2, 79% N_2) with nominal N_2O mole fractions of 300, 320 and 340 nmol mol^{-1} (BOC) were used as reference gases. These gas mixtures were compared with IMECC/NOAA standards to determine the exact values of (297.6 ± 0.1), (325.3 ± 0.1) and (344.2 ± 0.1) nmol mol^{-1} (NOAA-2006 scale). Reference gases and marine background air were measured twice a day for 20 min each during JR260B. Due to sufficient analyser stability during this cruise, calibration was reduced to once a day during JR255A/GENTOO. To ensure complete flushing of the cavity, only the last 5 min of each 20-min gas measurement were evaluated. Correspondingly, the first 15 min of equilibrator data following the reference gas and air measurements were discarded. Precision for single reference measurements (standard deviation of measurements at 1 Hz over 5 min) was 0.4 nmol mol^{-1}. The standard deviation of the uncorrected reference gas measurements throughout JR260B was 1.1 nmol mol^{-1} ($n = 29$) and 0.8 nmol mol^{-1} ($n = 19$) for JR255A/GENTOO. To estimate the long-term repeatability of the measurements after calibration, we used the standards with the lowest and highest N_2O mole fraction to calibrate the standard with the middle

N_2O mole fraction. The mean difference between resulting calibrated N_2O mole fraction and the actual value of 325.3 nmol mol^{-1} was (0.2 ± 0.1) nmol mol^{-1}, corresponding to a precision better than 0.1%. The flow rate of the headspace gas through the analyser was 400 mL min^{-1} (293 K, 1 bar) resulting in a 95% relaxation time ($t_{95} = 3\tau$) of approximately 7 min (*Grefe & Kaiser, 2014*). Data were acquired at a rate of 1 Hz; which were binned into 60 s averages for data evaluation purposes. Water flow through the equilibrator was held constant at 1.8–1.9 L min^{-1}, using a flow regulator ($\frac{1}{2}$ inch diameter tap tail flow regulator; Robert Pearson & Company Ltd, Warminster, UK). Water temperature in the equilibrator was measured with a Pt-100 temperature probe (Omega Engineering Limited, Manchester, UK), calibrated against a mercury reference thermometer to within $\pm 0.06\,°C$, and recorded using a RTD temperature recorder and USB Datalogger interface (both Omega Engineering Limited).

Concentration of dissolved N_2O (c) was calculated from the dry mole fraction measured in the equilibrator headspace (x), water temperature in the equilibrator (T_{eq}), salinity (S) and atmospheric pressure (p_{air}) using the solubility function F as described by *Weiss & Price (1980)*, Eq. (1).

$$c = xF(T_{eq}, S) p_{air}. \tag{1}$$

N_2O saturation in surface waters (s) was calculated by comparing x with the atmospheric mole fraction x_{air} and the respective equilibrium concentrations for (T_{eq}) and temperature at the seawater intake (T_{in}) Eq. (2).

$$s = \frac{xF(T_{eq}, S)}{x_{air} F(T_{in}, S)}. \tag{2}$$

Values for p_{air}, S and T_{in} were from the ship's surface water and meteorological monitoring system Surfmet (http://www.bodc.ac.uk).

Sea-to-air flux was calculated using wind speeds at 10 m above sea level from the CCMP Wind Vector Analysis Product (http://www.remss.com/measurements/ccmp). CCMP data have been interpolated to match cruise dates and positions for JR260B and JR255A/GENTOO. The gas transfer coefficient (k_w) was calculated, using the parameterisation of *Nightingale et al. (2000)* (Eq. (3)) and k_w was adjusted for N_2O with the Schmidt number Sc calculated following (*Wanninkhof, 2014*), Eq. (3).

$$\frac{k_w}{\text{m d}^{-1}} = 0.24 \left[0.222 \left(\frac{u_{CCMP}}{\text{m s}^{-1}} \right)^2 + 0.333 \frac{u_{CCMP}}{\text{m s}^{-1}} \right] \left(\frac{Sc}{600} \right)^{-0.5}. \tag{3}$$

The air-sea flux (Φ) was calculated from k_w and the difference between N_2O concentrations in seawater c and air saturation concentrations (c_{sat}), Eq. (4):

$$\Phi = k_w (c - c_{air}) = k_w \left[c - x_{air} F(T_{in}, S) p_{air} \right]. \tag{4}$$

Ship-based underway measurements of sea surface temperature and salinity were used to identify frontal structures for JR260B and JR255A/GENTOO. The location of these areas was then compared to the climatological front positions of *Orsi, Whitworth & Nowlin (1995)* to ensure positions based on measured salinity and temperature fall within expected geographical locations.

Satellite products for chlorophyll *a* and climatology data for nitrate (NO_3^-) concentrations were compared with *in situ* N_2O saturation data. Chlorophyll *a* concentrations were obtained from MODIS-Aqua (https://oceandata.sci.gsfc.nasa.gov) for December 2011 and January 2012. The level-3 product was downloaded at a 4 km resolution. Climatological mean dissolved NO_3^- concentrations were downloaded from the World Ocean Atlas 2013 (*Garcia et al., 2013*) for boreal winter (https://www.nodc.noaa.gov/OC5/woa13/woa13data.html). This climatology data was gridded 1° longitude by 1° latitude for 37 standard depths. Depth profiles taken during station work south of the PF and ACC for JR260B and JR255A/GENTOO respectively suggested a mixed layer depth (MLD) of approximately 60 m, similar to MLD derived from Argo float profiles January to March (*Dong et al., 2008*). NO_3^- concentrations from this depth were extracted from the climatology and interpolated along the cruise track for comparison with N_2O saturations.

RESULTS AND DISCUSSION

N_2O concentrations and saturations in the surface ocean

N_2O dry mole fractions measured in marine air were on average (323.6 ± 0.6) nmol mol^{-1} during JR260B and (324.0 ± 0.7) nmol mol^{-1} during JR255A/GENTOO. These values agree within measurement uncertainties with data from the Advanced Global Atmospheric Gases Experiment (AGAGE) for Cape Grim, Tasmania in January 2012 (40.68°S 144.69°E, (323.9 ± 0.5) nmol mol^{-1}). Surface water saturations and sea-to-air-flux were calculated based on the mean atmospheric mole fractions measured during JR260B and JR255A/GENTOO.
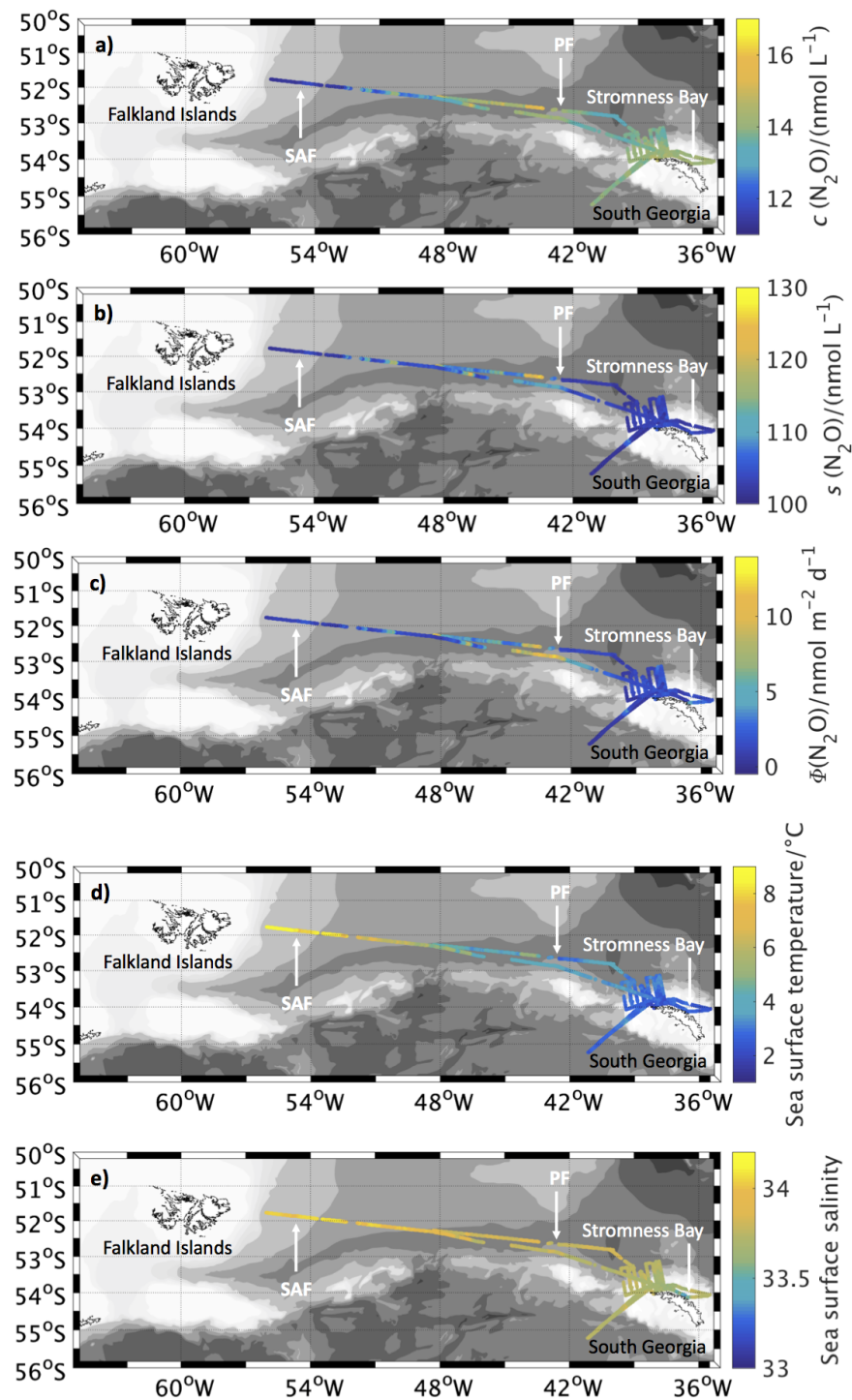
JR260B

Concentrations and saturations of N_2O in the surface ocean for JR260B are shown in Figs. 2A and 2B, respectively. Average N_2O concentrations were (14.0 ± 0.7) nmol L^{-1}, ranging from 11.2 nmol L^{-1} to 16.2 nmol L^{-1}. Average N_2O saturation was (104.3 ± 3.4)%, ranging from 99.4% to 126.1%.

For the purposes of the discussion of the data, they were divided into four different areas based on differences in biogeochemical conditions and oceanographic settings:

(a) Measurements between the Falkland Islands and the SAF in comparatively warm, saline surface waters (θ >7 °C, S 34.1–34.2) were located in the *Subantarctic Zone (SAZ)*.

(b) The *Polar Frontal Zone (PFZ)* covered the rapidly cooling and freshening surface waters (θ declining from 7 to 3 °C, S declining from 34.2 to 33.9) between the SAF and PF.

(c) The *Antarctic Zone (AAZ)* was identified by the relatively homogeneous cold and fresh *T*-*S* signature of AASW.

(d) *Stromness Bay* is discussed separately, due to the unique influence of the island of South Georgia in this area.

Subantarctic Zone (SAZ). In the Subantarctic Surface Waters (SASW) close to the Falkland Islands to the east of the Subantarctic Front (SAF), average surface concentrations were low, while saturations were similar to those observed in the Antarctic Zone (AAZ) (11.4 ± 0.2) nmol L^{-1}, (102.4 ± 0.7)%, see below). Water temperature and salinity were higher

Figure 2 **N$_2$O surface concentrations, saturations and fluxes, as well as sea surface temperature and salinity along cruise track for JR260B.** (A) N$_2$O concentration in surface waters along the cruise track of JR260B. (B) N$_2$O saturations calculated from measured atmospheric and seawater dry mole fractions. (C) Sea-to-air flux along the cruise track of JR260B. (D) Sea surface temperature and (E) salinity from underway measurements. Approximate position of Subantarctic Front (SAF) and Polar Front (PF) are indicated, based on sea surface temperature and salinity measurements during JR260B.

Full-size 🖼 DOI: 10.7717/peerj.5100/fig-2

than in the Antarctic waters south and east of the PF, so the difference in concentrations was mostly due to solubility effects. *Zhan & Chen (2009)* observed higher saturations (110 to 135%) to the north of the SAF in the Indian Sector of the Southern Ocean. The cause of this difference between the two sectors of the Southern Ocean is not known and highlights the need for more research to better understand marine N_2O cycling.

Polar Frontal Zone (PFZ). N_2O concentrations across the PFZ between the SAF and PF were highly variable with values ranging from 11.4 to 16.2 nmol L^{-1} (101.7 to 126.1% saturation) while water temperature and salinity were decreasing towards the east. Average concentrations and saturations across the PFZ were (13.8 ± 0.9) nmol L^{-1} and (108.8 ± 5.2)%, respectively.

The most important sources of N_2O to surface waters are upwelling of old water masses with preformed high N_2O concentrations and *in situ* production during remineralisation/nitrification or denitrification. High N_2O saturations across the PFZ could neither be attributed to a specific water mass (identifiable from temperature, salinity and density of the surface water), nor to a point on the mixing line between Subantarctic Surface Water (SASW) and Antarctic Surface Water (AASW) across the PFZ (Fig. 3A). Therefore, it is unlikely that upwelling and mixing processes or regional oceanographic features are the source of the high N_2O saturations across the PFZ.

Frontal systems can supply nutrients and iron to surface waters with large phytoplankton blooms forming across the PFZ, potentially fuelled by iron input from the Antarctic Peninsula archipelago, the Scotia Ridge and Georgia Rise (*De Baar et al., 1995*; *Wadley, Jickells & Heywood, 2014*). Satellite observations showed high chlorophyll *a* concentrations in proximity to high N_2O supersaturations in the PFZ (Fig. 4A, 'Comparison of N_2O surface saturations to chlorophyll a and nitrate concentration'). Remineralisation of sinking bloom biomass could lead to enhanced *in situ* N_2O production across the PFZ, resulting in high saturations.

In contrast to the high surface N_2O concentrations and saturations in the PFZ during JR260B, data from the Indian sector of the Southern Ocean showed minimum N_2O inventories within the PFZ (*Farías et al., 2015*). Farías et al. identify uptake of N_2O as an alternative substrate during biological nitrogen fixation as a potential sink process, presumably stimulated by iron input from the sediments of the Kerguelen archipelago. While both islands, South Georgia in the Atlantic and the Kerguelen Islands in the Indian Sector, are positioned within the PFZ and sediments are a source of iron to the water column, the data from the Kerguelen region were collected to the west of the islands, whereas JR260B data were collected to the east of South Georgia. The geographic location of the measurements in relation to islands could affect the biogeochemical properties of the water column and the community composition of N_2O cycling bacteria and archaea (*Santoro et al., 2011*; *Löscher et al., 2012*) and therefore result in major differences in the local source–sink behaviour of the ocean.

Antarctic Zone (AAZ). Average N_2O concentrations in the AAZ to the west of the PF near South Georgia were substantially higher than in the SAZ (14.1 ± 0.4) nmol L^{-1}. Saturations,
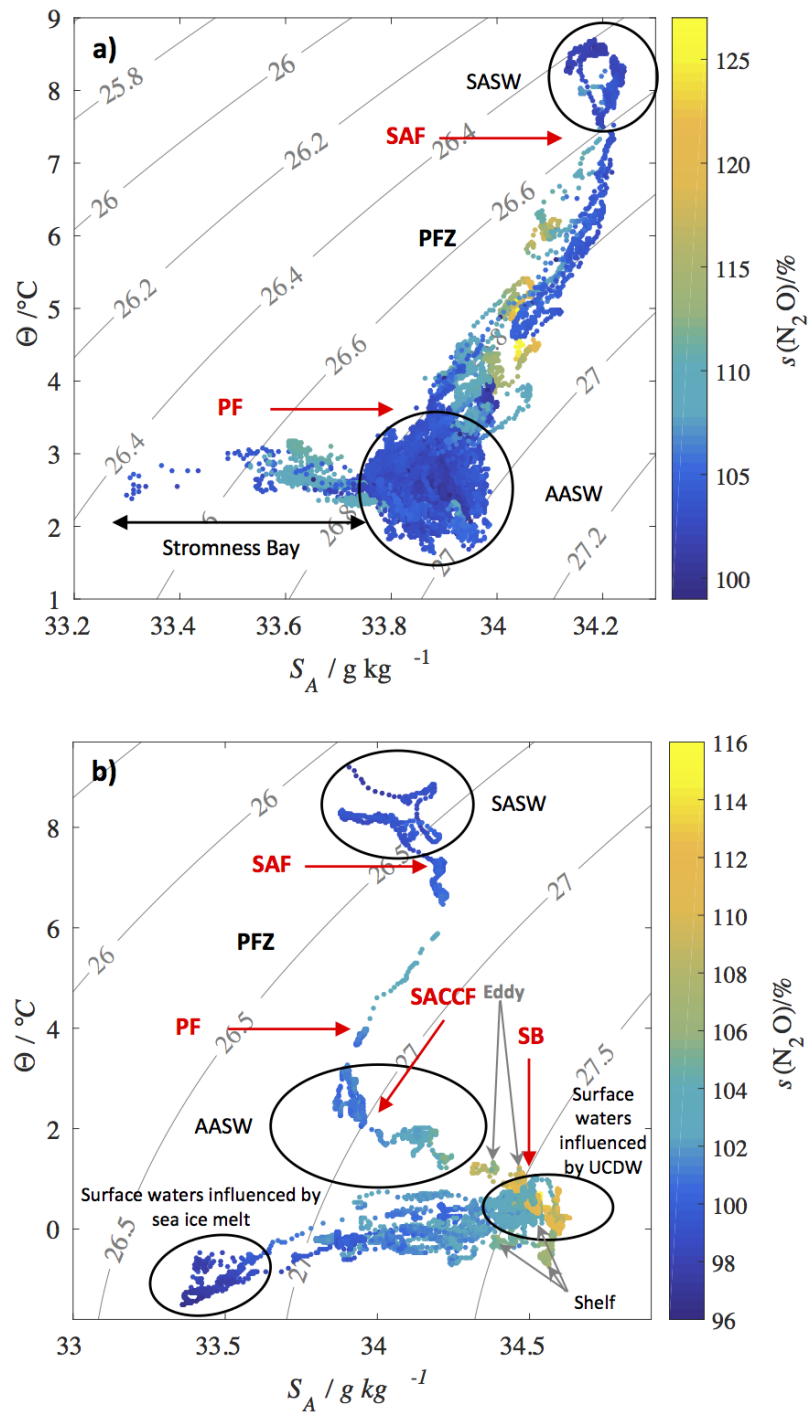
Figure 3 **N$_2$O saturations along potential density contours.** N$_2$O saturations s(N$_2$O) with corresponding absolute salinities S$_A$ and conservative temperatures Θ for (A) JR260B and (B) JR255A/GENTOO. Contour lines are the potential density anomalies (σ_θ) calculated using the TEOS-10 GSW toolbox (*McDougall & Barker, 2011*). Approximate positions of the Subantarctic Front (SAF), Polar Front (PF), Southern Antarctic Circumpolar Front (SACCF) and Southern Boundary of the Antarctic Circumpolar Current (SB) based on sea surface temperature and salinity measurements are indicated by red arrows. SASW, Subantarctic Surface Water; AASW, Antarctic Surface Water; UCDW, Upper Circumpolar Deep Water.

Full-size 🖾 DOI: 10.7717/peerj.5100/fig-3
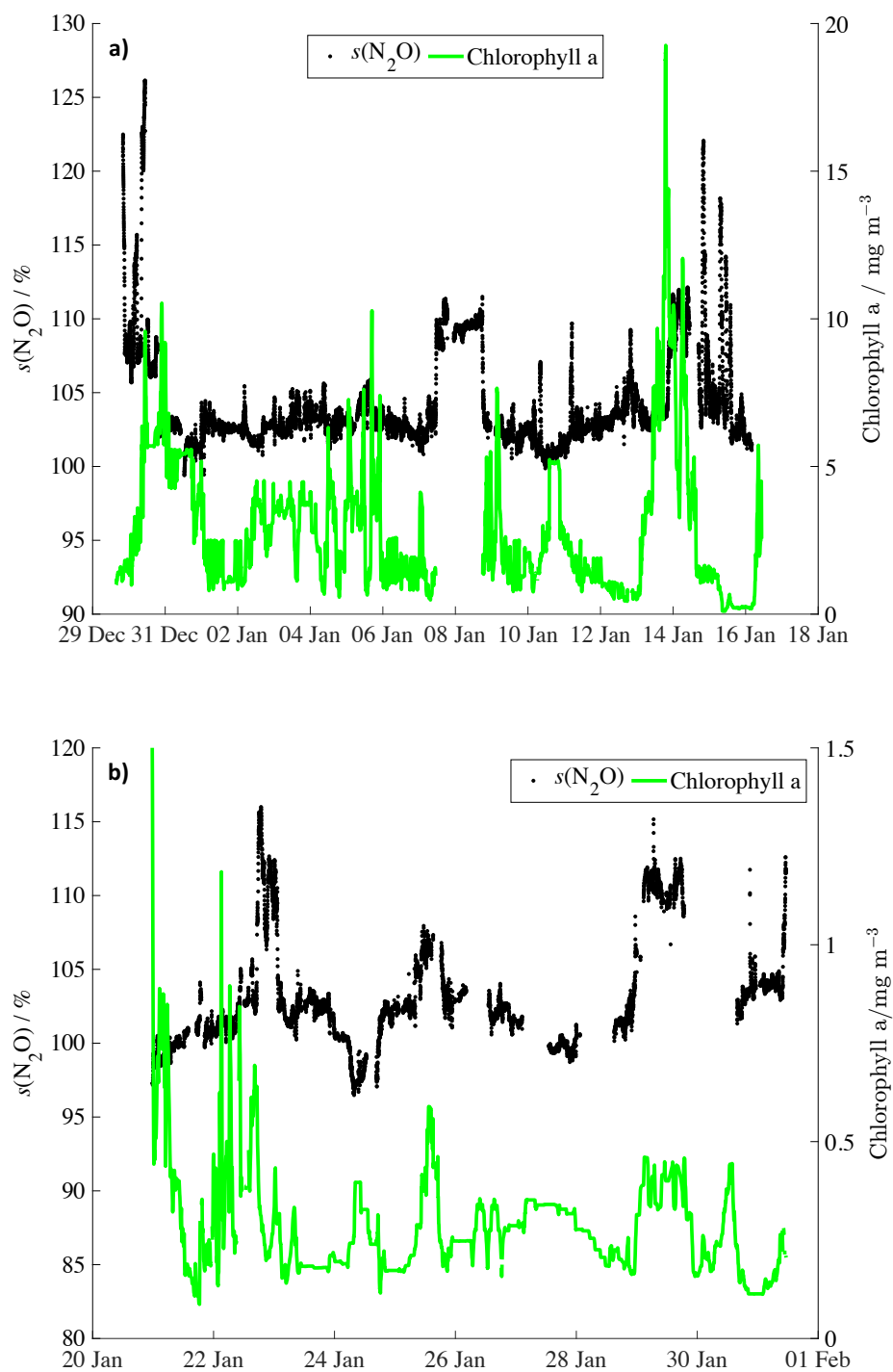
Figure 4 **N$_2$O saturations and chlorophyll concentrations for JR260B and JR255A/GENTOO.** Surface N$_2$O saturation during (A) JR260B (December 2011) and (B) JR255A/GENTOO (January 2012) in black and average chlorophyll concentrations from MODIS-Aqua in green. Due to cloud cover, there are no satellite data in the vicinity of South Georgia (8 Jan). The co-located s(N$_2$O) and c(Chl a) increases on 25 and 29 January correspond to the Antarctic shelf and the standing eddy (section 'JR255A/GENTOO'), respectively.

Full-size 🖼 DOI: 10.7717/peerj.5100/fig-4

however, were only slightly increased to $(103.9 \pm 3.1)\%$, similar to values of $(103.0 \pm 2.0)\%$ previously observed in the region (*Weiss et al., 1992*). The lower water temperature and salinity of Antarctic Surface Water AASW increased N_2O solubility, resulting in lower saturation values. Upwelling of deep water masses would not be expected away from the ACC and denitrification is not likely to take place in the oxygenated surface waters of the AAZ. Nitrification and nitrifier-denitrification would be more likely sources of *in situ* N_2O production. High nitrification rates (>30 mmol m^{-2} d^{-1}) were suggested for the Pacific sector of the Southern Ocean south of the PF (*Sambrotto & Mace, 2000*) and could also account for N_2O supersaturation observed in the AAZ of the Atlantic sector. Extensive phytoplankton blooms were observed in the vicinity of South Georgia and across the Scotia Sea, extending to the southern limit of the Polar Front (*Korb, Whitehouse & Ward, 2004*; *Korb et al., 2005*). These blooms can develop due to a stable water column over the shelf and iron input from the shelf sediments and island runoff (*De Baar et al., 1995*; *Holeton et al., 2005*; *Korb et al., 2005*; *Wadley, Jickells & Heywood, 2014*). This accumulation of biomass would supply ample substrate to sustain high nitrification rates and N_2O production could lead to the observed supersaturation close to the island, despite the absence of a clear correlation between chlorophyll a, climatological NO_3^- concentrations and N_2O saturations ('N_2O sea-to-air flux'). Not much is known about nitrifier-denitrification in polar waters and additional research is required to estimate the importance of this production pathway for N_2O accumulations in surface waters.

Stromness bay. N_2O concentrations and saturations in coastal Stromness Bay, South Georgia, were higher than in the open waters of the AAZ ((14.8 ± 0.3) nmol L^{-1} and $(108.1 \pm 2.6)\%$, respectively) with highest saturations observed where fresh meltwater runoff from the island was mixing with AASW (Fig. 3A). Terrestrial runoff can transport iron and biomass from land into the sea and stimulate productivity and subsequent remineralisation where N_2O is produced during nitrification. In addition, fur seals (*Arctocephalus gazella*) and macaroni penguins (*Eudyptes chrysolophus*) have large breeding colonies on South Georgia, re-distributing nitrogen from their hunting grounds to the island (*Whitehouse et al., 1999*).

While no NO_3^- concentrations are available for JR260B, *Rees et al. (2016)* observed high NO_3^- values of 25.8 µmol L^{-1} at the base of the mixed layer north of South Georgia in austral summer 2013. Concentrations would be expected to be even higher in Stromness Bay due to land run-off and the high abundance of penguins and seals observed at the shore and in the water at the time of measurements. High nitrogen loads in coastal waters are expected to lead to high N_2O saturations (*Bange, Rapsomanikis & Andreae, 1996*) and would explain the consistently high supersaturations observed in Stromness Bay during JR260B.

Nitrifier-denitrification in anoxic sites of suspended particles can be an additional source of N_2O (*Ostrom et al., 2000*). As the water depth in Stromness Bay is shallow (60 m) and well mixed at the anchoring site, N_2O produced by denitrification at the sediment interface could have diffused into the water column, contributing to the high concentration at the surface.

JR255A/GENTOO

During JR255A/GENTOO, average N_2O surface concentrations were (14.9 ± 1.2) nmol L^{-1}, corresponding to saturations of $(103.1 \pm 3.6)\%$ (range: $(10.6–17.0)$nmol L^{-1}; $(96.5–116.0)\%$ saturation). While N_2O concentrations were higher than for JR260B, mainly due to the lower water temperatures, average saturations were slightly lower.

As for JR260B, data have been discussed for three areas, based on substantial differences in biogeochemical conditions and oceanographic settings:

(a) Data collected between the Falkland Islands and the South Scotia Ridge were discussed below as *Drake Passage*, crossing the SAF ($\theta > 7$ °C to the north), PF (θ decreasing from 7 °C to 3 °C, S from 34.2 to 33.8), SAACF (identified by a small salinity change in surface waters from 33.8 to 34) and SB (surface waters influenced by UCDW, S increases from 34.4 to 34.6);

(b) South of the South Scotia Ridge, measurements were designated as *Weddell Sea* data, including a standing eddy (identified by a decrease in surface salinity from 34.4 to 34.2 and an increase of surface temperature at the edges from 0.5 to 1 °C, *Thompson et al., 2009*) forming over the ridge and data collected from the Antarctic shelf;

(c) Measurements influenced by the *sea ice edge* in the Weddell Sea ($\theta < 0$ °C and salinity < 33.6).

Drake Passage. Average N_2O concentrations at the beginning of the cruise were (13.7 ± 1.8) nmol L^{-1} $((102.9 \pm 4.2)\%$ saturation). Decreasing temperatures during transit across Drake Passage to the Eastern Antarctic Peninsula partially accounted for increasing N_2O concentrations (Fig. 5A), resulting in a wide range of concentrations across the region, whereas saturations were on average only slightly above equilibrium with the atmosphere. Water masses across the Drake Passage were Subantarctic Surface Water to the north of the SAF and Antarctic Surface Water to the south of the PF (SASW and AASW, respectively) (Fig. 3B). As these surface waters are in constant contact with the atmosphere, they are expected to be in equilibrium with the atmosphere in absence of biological N_2O sources. N_2O saturations above 100% would therefore be due to *in situ* production during remineralisation of biomass.

For comparison, *Rees, Owens & Upstill-Goddard (1997)* observed slightly lower saturations for Drake Passage $((99.7 \pm 3.0)\%)$, while *Weiss et al. (1992)* reported values close to the data presented here (Ajax 2: $(102.3 \pm 0.9)\%$, JR255A/GENTOO: $(102.9 \pm 4.2)\%)$. Higher saturation values for *Weiss et al. (1992)* and JR255A/GENTOO could be due to interannual and seasonal variability. JR255A/GENTOO and Ajax 2 took place in January and February, later in the austral summer season than the November/December cruise of *Rees, Owens & Upstill-Goddard (1997)*. Nitrification as part of the remineralisation of sinking biomass could have increased N_2O accumulations in the mixed layer over the summer, resulting in higher values later in the growing season. No direct link to chlorophyll *a* concentrations was found ('Comparison of N_2O surface saturations to chlorophyll a and nitrate concentrations'), and was unlikely to exist due to the temporal and spatial decoupling.
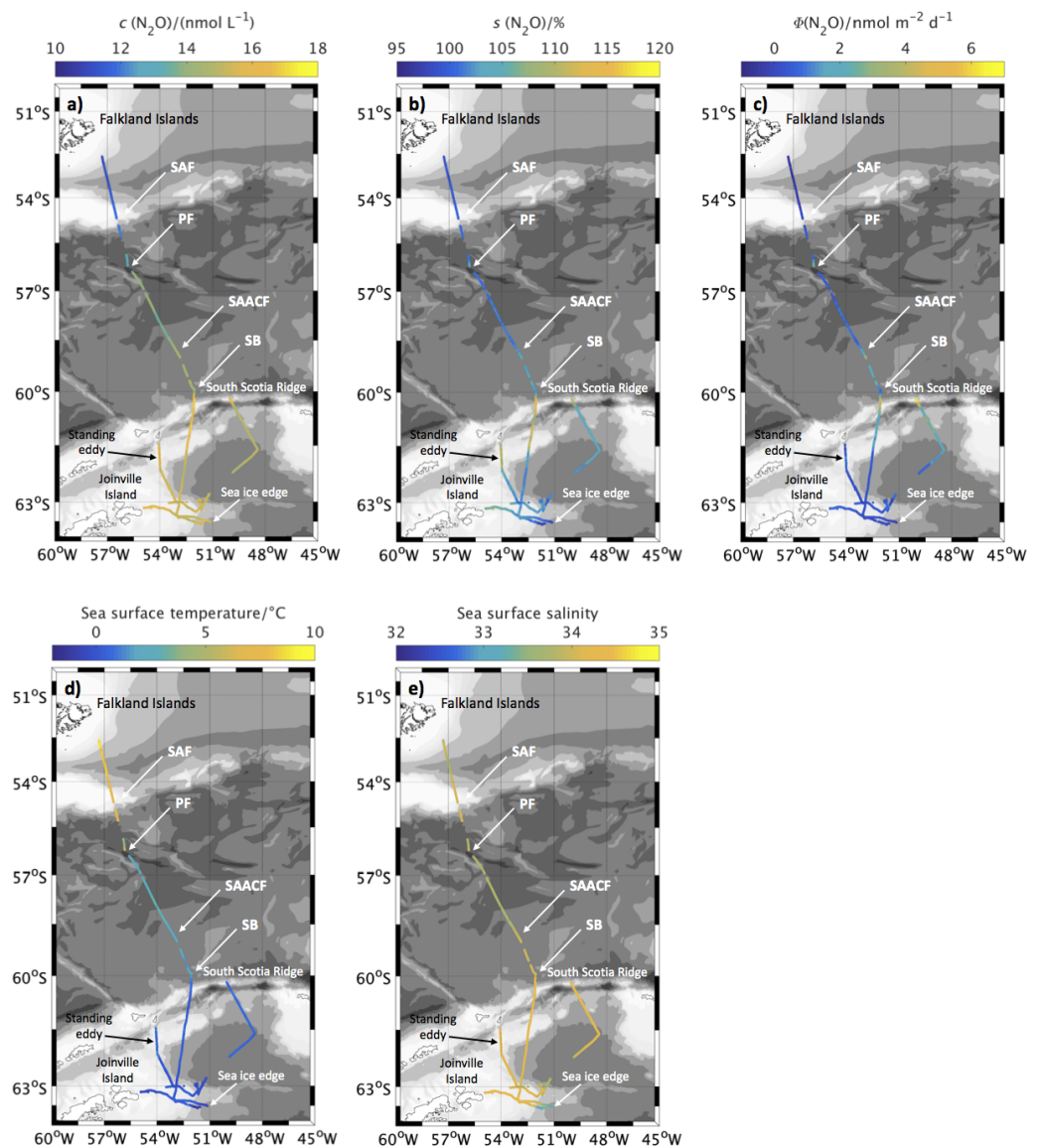
Figure 5 **N$_2$O surface concentrations, saturations and fluxes, as well as sea surface temperature and salinity along cruise track for JR255A.** (A) N$_2$O concentration in surface waters along the cruise track of JR255A. (B) N$_2$O saturations calculated from measured atmospheric and seawater dry mole fractions. (C) Sea-to-air flux along the cruise track of JR255A. (D) Sea surface temperature and (E) salinity from underway measurements. Approximate position of Subantarctic Front (SAF), Polar Front (PF) and Southern Boundary (SB) are indicated, based on sea surface temperature and salinity measurements during JR255A.

Full-size ☒ DOI: 10.7717/peerj.5100/fig-5

Just south of the Southern Boundary of the Antarctic Circumpolar Current (SB), concentrations as well as saturations reached the highest values observed during JR255A/GENTOO. Temperature and salinity characteristics of the surface water indicated an influence of Upper Circumpolar Deep Water (UCDW) from below (Fig. 3B, *Orsi, Whitworth & Nowlin, 1995*). UCDW is an old water mass, high in remineralised nutrients and N$_2$O as a byproduct of nitrification. Depth profiles in the Indian sector of the Southern

Ocean displayed N_2O maxima in the oxygen minimum layer of the UCDW and potential transport of these waters to the surface (*Chen et al., 2014*; *Zhan et al., 2015*). Entrainment of UCDW across the thermocline, as inferred from a decrease in surface temperature and an increase in salinity, could explain the high saturations across the SB during JR255A/GENTOO. Additionally, iron input from the Scotia Ridge, as observed by *Klunder et al. (2014)* could enhance *in situ* productivity, supplying substrate in form of sinking particles for *in situ* N_2O production.

Weddell sea. Surface N_2O concentrations of the open waters of the Weddell Sea were on average (15.2 ± 0.2) nmol L^{-1} $((102.2 \pm 1.6)\%$ saturation). South of the ACC, the surface waters were colder than across Drake Passage, increasing the solubility of N_2O and resulting in slightly lower saturations despite higher concentrations. Small but persistent supersaturations during JR255A were in contrast to N_2O data from the Indian sector, where surface waters were mainly undersaturated (*Chen et al., 2014*; *Zhan & Chen, 2009*; *Zhan et al., 2015*). Meltwater low in N_2O in combination with strong stratification, preventing exchange across the thermocline were identified as possible reasons for N_2O undersaturations. While underaturations were observed during JR255A/GENTOO close to the sea ice edge (see below), meltwater does not seem to have a strong impact on the N_2O saturations of surface waters in the Weddell Sea. Further studies are required to identify the differences between the Atlantic and Indian sector of the Southern Ocean in terms of meltwater contribution to the mixed layer and strength of stratification and mixing across the thermocline.

Higher-than-average N_2O saturations for the Weddell Sea during JR255A/GENTOO were observed on the Antarctic shelf off the tip of Joinville Island $((104.2 \pm 1.7)\%)$ and during the section across the large standing eddy forming over the South Scotia Ridge, centred on 62°S and 54°W (*Thompson et al., 2009*) $((110.5 \pm 1.2)\%)$ (Figs. 5A and 5B). Iron from the sediments, as well as land run-off could have stimulated productivity in these areas (*Klunder et al., 2014*; *Sañudo Wilhelmy et al., 2002*; *Thompson & Youngs, 2013*; *Wadley, Jickells & Heywood, 2014*). In addition, the sampling region was more sheltered from the circumpolar winds by the Antarctic Peninsula, stabilising the water column over the shallow bathymetry. The combination of ample supply of trace nutrients and a stable water column, keeping phototrophic organisms in the euphotic zone, presumably resulted in comparably high productivity and subsequent N_2O production during remineralisation of sinking biomass. In the vicinity of dynamic features, such as frontal zones, average chlorophyll concentrations for January 2012 show an increase in chlorophyll a over the shelf and across the standing eddy where N_2O saturations are highest (Fig. 4: 25 and 29 Jan). In areas where physical transport and mixing is reduced, N_2O, as well as chlorophyll, can accumulate and show the expected relationship between high productivity and N_2O production during nitrification as sinking biomass is remineralised.

Sea ice edge. Lowest saturations of on average $(98.8.0 \pm 1.3)\%$ were observed close to the sea ice edge in the south east of the survey region (Fig. 5B). Average N_2O concentrations at the ice edge were (15.2 ± 0.2) nmol L^{-1}, similar to the average of (15.4 ± 0.2) nmol L^{-1}

observed in the other open ocean regions in the Weddell Sea. Saturations, however, were lower due to lower temperature and salinity, resulting in higher N_2O solubility. *Randall et al. (2012)* observed under-saturations of N_2O within sea ice due to loss of dissolved gases during brine rejection. Mixing of seawater with under-saturated melt water from sea ice that has undergone brine rejection during formation would decrease surface concentrations, which was not observed during JR255A. However, it is possible that end-members were not captured in these measurements and the mixing line for temperature and salinity indeed indicates dilution of Weddell Sea surface waters with melt water low in N_2O.

Comparison of N_2O surface saturations to chlorophyll a and nitrate concentrations

Satellite products and climatologies are readily available datasets, covering pigment and nutrient distribution for wide areas of the global ocean. To investigate potential links of N_2O surface saturations to productivity and remineralisation, we have tried to find correlations between N_2O, chlorophyll *a* concentrations (as proxy for biomass accumulation) and nitrate concentrations (as proxy for integrated remineralisation). A tentative link between chlorophyll *a* concentrations from satellite products and NO_3^- concentrations from climatologies could also open up these data sources to infer global and long-term N_2O saturations without relying on *in situ* data or N_2O models.

Surface saturations of N_2O were compared to monthly average chlorophyll *a* concentration for December 2011 and January 2012 (Figs. 5 and 6). There was no simple correlation between N_2O saturations and chlorophyll *a* concentrations, neither for specific areas of the two cruises, nor for the complete dataset (Figs. 6A and 6B). However, average chlorophyll was high in proximity to the crossings of the PFZ during JR260B (Fig. 4A: 30 Dec, 15 Jan).

In addition to satellite chlorophyll values, NO_3^- concentrations from the World Ocean Atlas climatology (https://www.nodc.noaa.gov/OC5/woa13/woa13data.html) were calculated for the mixed layer (MLD, 60 m) and were compared to N_2O saturations for JR260B and JR255A/GENTOO to test whether NO_3^- as end-product of nitrification could be used as a proxy for mixed layer N_2O production (Figs. 7A and 7B). However, again no clear correlation was observed between N_2O saturations and NO_3^- concentrations, neither for specific survey areas and oceanographic features, nor for the entire dataset.

Chlorophyll as a proxy for productivity and NO_3^- as the endproduct of nitrification (a major N_2O-producing pathway) might be expected to show similar behaviour to N_2O mixed layer saturations. However, there are reasons why we do not observe simple correlations between these parameters.

Firstly, there is the methodological issue of comparing near real-time N_2O data with monthly averages (chlorophyll) and climatology data (NO_3^-). The location of frontal systems and upwelling water masses in the Southern Ocean are not fixed. Mixing and transport of water will influence observations during JR260B and satellite and climatology data.

Secondly, biomass (represented by chlorophyll) is not immediately available to nitrifying organisms. Breaking down of sinking biomass and release of NH_4^+, the substrate for nitrification, introduces a time delay for N_2O production. NH_4^+ and NO_3^- are not
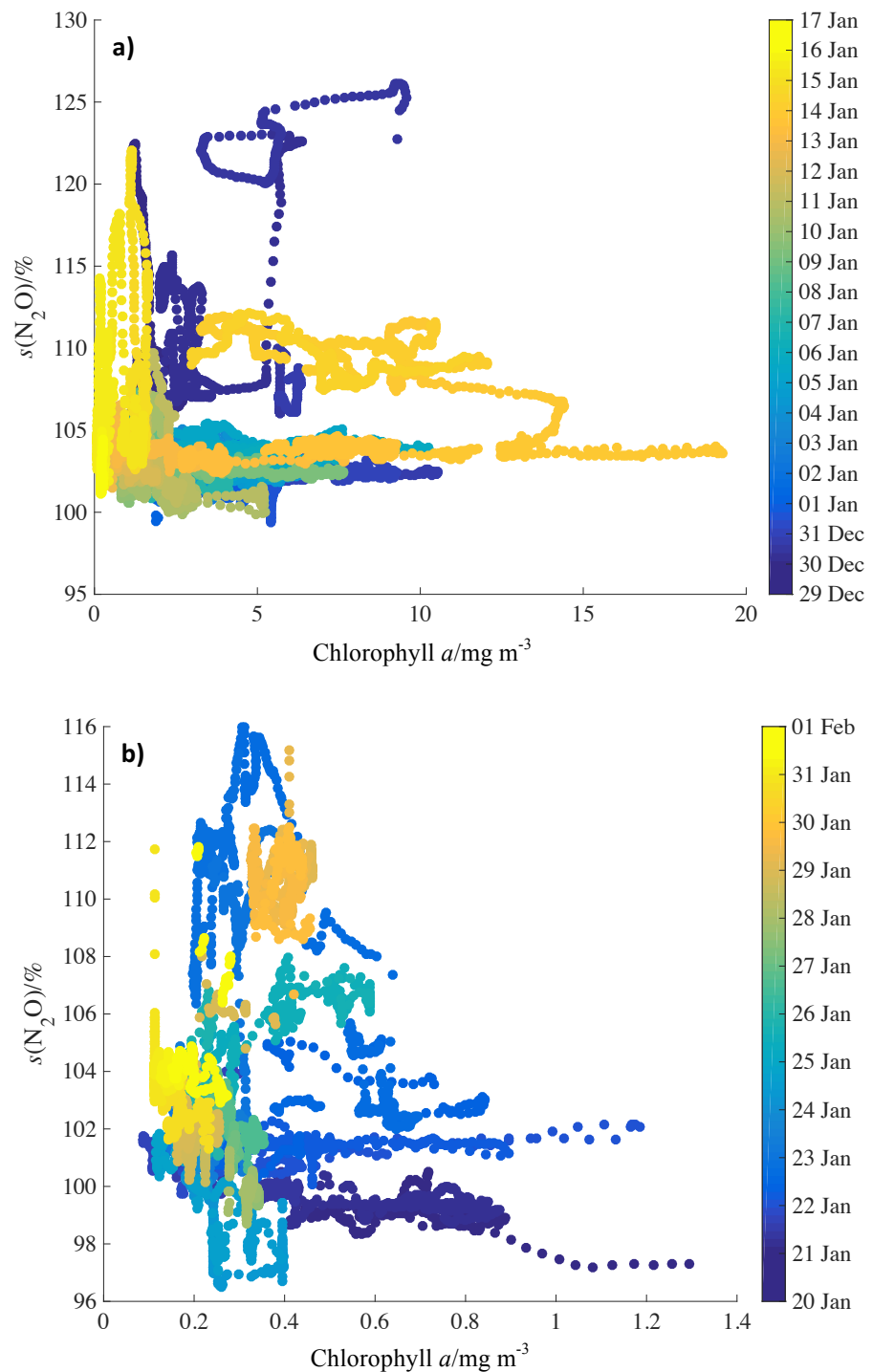
Figure 6 **Relationship of N₂O saturations to chlorophyll concentrations by date.** N$_2$O saturations during (A) JR260B (December 2011) and (B) JR255A/GENTOO (January 2012) plotted against average satellite chlorophyll concentrations for December 2011 from MODIS Aqua. Symbols are colour-coded for date. Note the different axis scales.
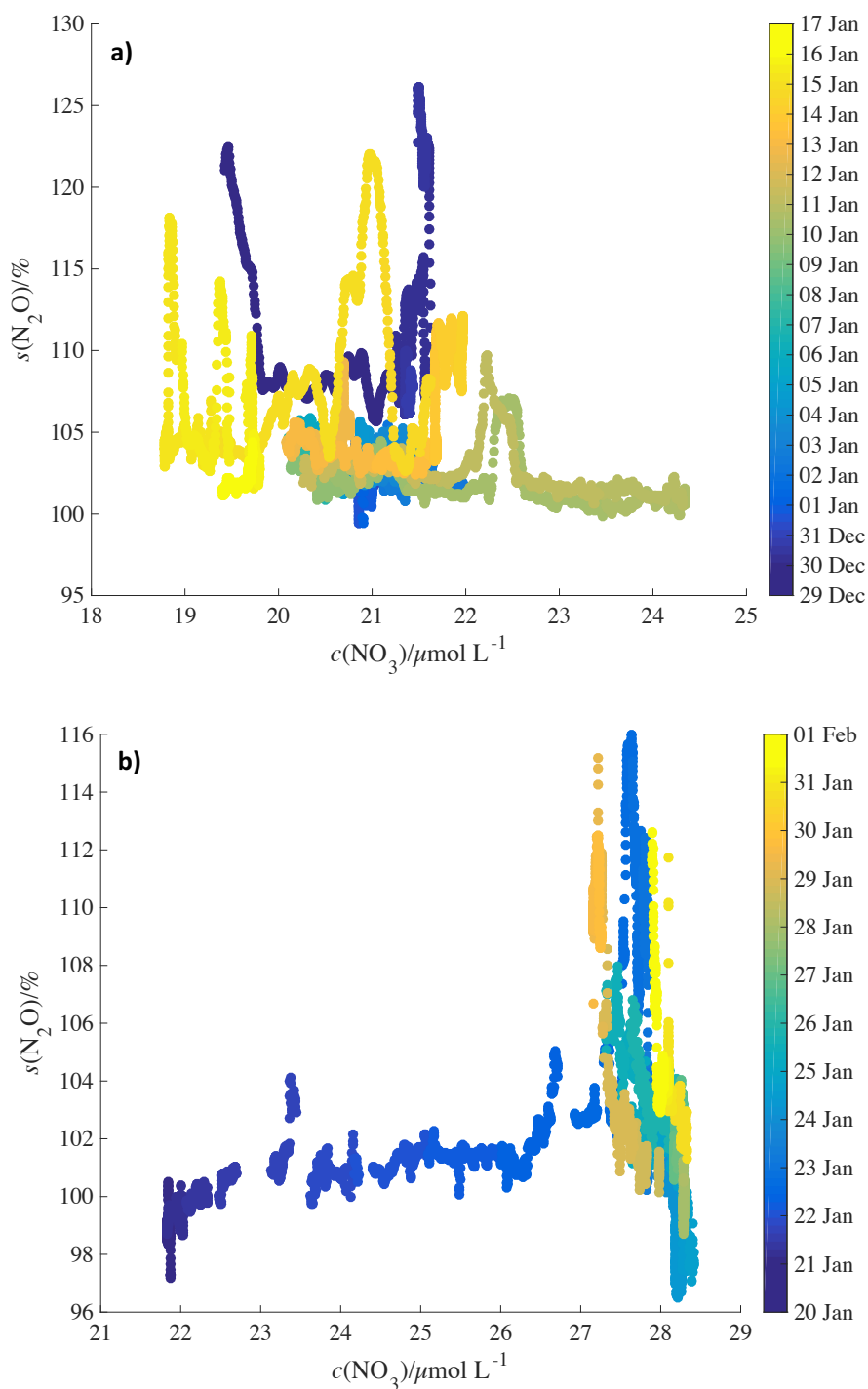
Figure 7 **Relationship between N$_2$O saturations and MLD NO$_3^-$ concentrations by date.** N$_2$O saturations (A) during JR260B and (B) JR255A/GENTOO plotted against mean winter MLD NO$_3^-$ concentrations from World Ocean Atlas. Symbols are colour-coded for date.

Full-size 🖼 DOI: 10.7717/peerj.5100/fig-7

exclusively controlled by the activity of nitrifying bacteria and archaea. They are also important nutrients for phytoplankton, therefore uptake by algae is further complicating the use of NO_3^- as a proxy for N_2O saturations.

The lack of a clear, quantitative link between N_2O saturations and observations of chlorophyll a and NO_3^- makes it difficult to infer $s(N_2O)$ (unlike CO_2) by multi-linear regression (*Wallace, 1995*) or prognostic neural network models (*Landschützer et al., 2014*). Despite the absence of a quantitative correlation, high N_2O saturations were accompanied by an increase in chlorophyll a concentrations on the Antarctic shelf and across the standing eddy.

N_2O sea-to-air flux

Sea-to-air flux during JR260B and JR255A/GENTOO was calculated as described above. For comparison to global average sea-to-air flux, a global ocean area of 361.9×10^6 km^2 was used (*Eakins & Sharman, 2010*). Oceans contribute approximately 25% to global N_2O emissions of 17.9 Tg a^{-1} (N equivalents) (*Ciais et al., 2013*), resulting in a marine source of 4.5 Tg a^{-1} or 4.4×10^8 mol d^{-1}. This results in an average sea-to-air flux of 1.2 µmol m^{-2} d^{-1} for the global ocean. For comparison, *Nevison, Weiss & Erickson (1995)* estimated a global oceanic N_2O source of 4 Tg a^{-1}, resulting in a slightly lower average flux of 1.08 µmol m^{-2} d^{-1}.

JR260B

Surface waters during JR260B were mainly a source of N_2O to the atmosphere (Fig. 2C). The average flux of 2.2 µmol m^{-2} d^{-1} was almost twice the global average flux of 1.2 µmol m^{-2} d^{-1}, based on *Ciais et al. (2013)*.

The average sea-to-air flux within the SAZ was (1.1 ± 0.4) µmol m^{-2} d^{-1}, due to low to moderate wind speeds at the time of measurements and saturations just slightly above equilibrium with the atmosphere. The data from the SAZ were limited to the very beginning and very end of each transit to the Scotia Sea and Weddell Sea, therefore the flux values presented here might not be representative of the wider SAZ. Despite the proximity to the Falkland Islands, no enhancing island effect on N_2O saturations and flux was observed (in comparison to South Georgia). While this work is focussed on emissions across the ACC and south of the SB, more data are required from subpolar regions for a better understanding of oceanic N_2O sources.

N_2O flux progressively increased across the PFZ to an average of (3.6 ± 2.4) µmol m^{-2} d^{-1} with highest values of 13.2 µmol m^{-2} d^{-1} during transit from South Georgia back to the Falkland Islands. Average global flux values were highly exceeded across the frontal zone as high N_2O supersaturations, possibly a result of *in situ* production due to high biomass supported by iron supply from sediments, coinciding with high circumpolar wind speeds. As these high emissions were not observed during the crossing of the PFZ further to the west during JR255A/GENTOO (see below), it would be important to find out if this is a local phenomenon, influenced for example by the deflection of the ACC around South Georgia, or if the PFZ is a strong source of N_2O to the atmosphere in other sectors of the Southern Ocean. Bathymetry might be a controlling factor as a source of iron to the water column, supporting productivity and subsequent N_2O production during remineralisation (*Wadley, Jickells & Heywood, 2014*).

Sea-to-air flux decreased again in the open waters of the AAZ around South Georgia as N_2O supersaturations were lower. The average flux of (1.8 ± 1.8) μmol m^{-2} d^{-1} was, however, still exceeding the global average. As productivity in the Scotia Sea is higher than in other HNLC areas of the Southern Ocean, these high fluxes might be restricted to similar areas where islands presumably enhance productivity and N_2O emissions. Negative flux up to -0.5 μmol m^{-2}d^{-1} was only observed in a small area to the east of the PF during transit to South Georgia. It was not apparent what caused this localised and potentially transient sink; uptake by nitrogen fixing bacteria might be a possible mechanism for loss of N_2O from surface waters (*Farías et al., 2015*).

In contrast to the open waters of the AAZ, Stromness Bay was a strong source of N_2O to the atmosphere while the ship was anchored for calibration of acoustic instruments. Sea-to-air flux was initially only slightly higher than for the surrounding open ocean area (2.2 μmol m^{-2} d^{-1}), despite high N_2O supersaturations in the bay (on average around 108.1%). This was due to low wind speeds of 7.3 m s^{-1}, which subsequently increased to 14.5 m s^{-1} over 25 h, resulting in sea-to-air fluxes of up to 10.6 μmol m^{-2} d^{-1} and an average of (4.5 ± 2.4) μmol m^{-2} d^{-1}. These observations highlight the impact of island productivity, as well as changes in the weather/wind speed for N_2O emissions from the ocean. While the coastal region of South Georgia only accounts for a small surface area of the Scotia sea, emissions are very high. If this effect could be observed across other island systems in the Southern Ocean, the cumulative effect might be of significance for global flux estimates. Sea-to-air flux was controlled by increasing wind speed (saturations were stable for the 25 h observation period), which highlights the impact of changes to the climate system for the source strength of regions with high surface N_2O saturations. This is of particular importance for the Southern Ocean where an increase in wind speed is expected for the future (*Young, Zieger & Babanin, 2011*; *Hande, Siems & Manton, 2012*).

Overall, the surface ocean across the Scotia Sea was a strong source of N_2O to the atmosphere for most of the research cruise JR260B with sea-to-air fluxes exceeding global average flux. These high fluxes were driven by high surface water saturations, presumably resulting from *in situ* production, and moderate to high wind speed.

JR255A/GENTOO

The average sea-to-air N_2O flux throughout JR255A/GENTOO was (0.6 ± 0.9) μmol m^{-2} d^{-1}, which is below global average values of 1.2 μmol m^{-2} d^{-1} and considerably lower than the average flux for JR260B, just to the north of the JR255A/GENTOO region. The low flux was a result of lower saturation values compared with JR260B, but still above equilibrium with the atmosphere for most of the cruise. Additionally, wind speeds were lower during JR255A/GENTOO.

The highest sea-to-air flux of 6.7 μmol m^{-2} d^{-1} was observed across the South Scotia Ridge where high wind speeds coincided with high N_2O supersaturations, presumably due to surface waters being influenced by underlying UCDW high in N_2O. For a better estimate of Southern Ocean N_2O emissions, it would be important to investigate the circumpolar source strength of N_2O along the SB where UCDW is expected to influence the SML. In combination with potentially increasing wind speed in the Southern Ocean (*Young, Zieger*

& *Babanin, 2011*; *Hande, Siems & Manton, 2012*), the SB could be a substantial source of N_2O to the atmosphere.

Although surface waters were most strongly undersaturated at the sea ice edge, negative fluxes were highest at the beginning of the cruise, close to the Falkland Islands (-1.3 µmol $m^{-2} d^{-1}$). Highest wind speeds of up to 13.3 m s^{-1} were observed at that time, driving the strong negative fluxes on the shelf. At the ice edge, in contrast, wind speeds were considerably lower (1.4 to 6 m s^{-1}), resulting in weaker negative fluxes. The underlying mechanism for undersaturation on the Falkland shelf is currently unknown, but might be related to seasonal heat fluxes/cooling of the surface ocean, which occurs on faster time scales than air-sea gas exchange. Similar to localised negative fluxes during JR260B, uptake of N_2O as an alternative substrate during biological nitrogen fixation could also be a sink (*Farías et al., 2015*).

N_2O sinks at the sea ice edge are most likely controlled by physics by increasing solubility in cold, fresh waters or by N_2O drawdown through brine rejection (*Randall et al., 2012*). Physical drawdown of N_2O could buffer the atmospheric increase, but water high in N_2O would nevertheless eventually find its way back into the surface mixed layer. The impact of the sea ice edge sink on oceanic N_2O emissions is currently not very well understood and requires further observations, as well as integration into emission models.

Low wind speeds also affected sea-to-air flux on the Antarctic shelf close to Joinville Island, as well as across the standing eddy over the South Scotia Ridge. Despite relatively high supersaturations, N_2O flux was rather low ((0.4 ± 0.2) and (0.5 ± 0.4) µmol m^{-2} d^{-1}, respectively). As the data collected during JR255A/GENTOO only present a snapshot of N_2O saturations and resulting sea-to-air flux, shelf areas and eddies might contribute more strongly to global emissions at other times. Productivity is expected to be high throughout the summer months, and a change in weather and wind speed could substantially increase the source strength of these areas (see JR260B, Stromness Bay above). Again, additional data throughout the year, as well as from other sectors of the Southern Ocean, are required to better understand the strength and variability of N_2O emissions. Regional biogeochemical and emission models might be helpful to elucidate the links between productivity, dominant nitrogen and N_2O cycling pathways and changing weather conditions to improve estimates for the Southern Ocean source strength.

Throughout JR255A/GENTOO sea-to-air flux of N_2O was low compared to JR260B, as well as the global average, mainly due to low wind speed rather than low N_2O saturation of surface waters. The continental shelf and oceanographic features like eddies hold the potential for substantial N_2O sources if wind speed increases and production in the water column is sustained.

CONCLUSIONS

High-resolution (1 min averages of measurements at 1 Hz) N_2O data were collected from the surface waters of the Atlantic sector of the Southern Ocean during transit and station work, covering highly varied areas across the ACC and the AAZ. These data from the austral summer 2011/2012 add substantially to the limited observations of N_2O emissions from

the Southern Ocean, increasing observations from the Scotia Sea by 20,674 values (188 data points from 1989 previously published by *Weiss et al. (1992)*) and by 9730 from the Weddell Sea (250 data points from 1984 previously published by *Weiss et al. (1992)*), and show unprecedented fine-scale variability compared to the existing data (supplementary Figures 1 and 2 in *Weiss et al., 1992*).

Both, the Scotia Sea and the Weddell Sea, were a source of N_2O to the atmosphere. The source strength was highly variable in space and time with rare areas of negative sea-to-air flux.

The following areas were identified as strong N_2O sources by high sea-to-air flux at the time of the survey and/or high supersaturations:

- shallow bathymetry/ridges: North and South Scotia Ridge,
- shelf and coastal areas: The Antarctic shelf and coastal South Georgia and
- the Polar Frontal Zone: To the east of Drake Passage,

whereas N_2O sources were associated with water mass transport at

- the Southern Boundary of the ACC, where shoaling UCDW was influencing surface waters of the mixed layer.

The following areas were identified as sinks for atmospheric N_2O by negative sea-to-air flux at the time of the survey:

N_2O sinks through physical processes:

- Sea ice edge: N_2O sink due to increased solubility or brine rejection.

N_2O sinks through other processes, presumably seasonal cooling and temporal lag between heat and gas fluxes and/or biological nitrogen fixation:

- Falkland shelf to the south of the islands.
- To the east of the PF in the Scotia Sea.

Neither chlorophyll *a*, nor NO_3^- concentrations showed any correlation to N_2O saturations. Assuming that the average flux values of 2.3 μmol m^{-2} d^{-1} and 0.7 μmol m^{-2} d^{-1} calculated for JR260B and JR255A are representative for the Scotia Sea and Weddell Sea over time, the combined area would contribute 0.04 Tg a^{-1} N (nitrogen equivalent) to the global N_2O source. While this value is relatively low, also compared to model estimates of 0.9 Tg a^{-1} N (nitrogen equivalents) for the entire Southern Ocean (*Nevison et al., 2005*), areas with a strong variability in N_2O saturation and sea-to-air flux were observed for both cruises. Short-term average flux for the Scotia Sea was almost twice as high as the global average. These findings indicate the importance of high-resolution data to accurately estimate the source strength of mesoscale features, such as frontal systems and eddies. This study highlights the need for further high-resolution data from other sectors of the Southern Ocean to resolve variability in N_2O emissions and improve global emission estimates.

ACKNOWLEDGEMENTS

We would like to thank two anonymous reviewers and the editor for their helpful comments which greatly improved the manuscript. Thanks to the officers and crew on board RRS James Clark Ross and the scientific party for their support during JR260B and JR255A/GENTOO. We also thank Sunke Schmidtko for supplying calibrated sea surface temperature and salinity, Dorothee Bakker for providing the equilibrator used in this study and Gareth A. Lee for technical support. N_2O data from *Weiss et al. (1992)* was downloaded from the MEMENTO database (https://memento.geomar.de/; *Kock & Bange, 2015*).

ADDITIONAL INFORMATION AND DECLARATIONS

Competing Interests

Jan Kaiser is an Academic Editor for PeerJ.

Author Contributions

- Imke Grefe conceived and designed the experiments, performed the experiments, analyzed the data, contributed reagents/materials/analysis tools, prepared figures and/or tables, authored or reviewed drafts of the paper, approved the final draft.
- Sophie Fielding and Karen J. Heywood analyzed the data, contributed reagents/materials/analysis tools, authored or reviewed drafts of the paper, approved the final draft.
- Jan Kaiser conceived and designed the experiments, analyzed the data, contributed reagents/materials/analysis tools, authored or reviewed drafts of the paper, approved the final draft.

Data Availability

The following information was supplied regarding data availability:

Data has been deposited at the MEMENTO database (MarinE MethanE and NiTrous Oxide) and is available upon request: https://memento.geomar.de/database. Data can also be found in the Supplemental Information.

Supplemental Information

Supplemental information for this article can be found online at http://dx.doi.org/10.7717/peerj.5100#supplemental-information.

REFERENCES

Arevalo-Martinez DL, Beiyer M, Krumbholz M, Piller I, Kock A, Steinhof T, Körtzinger A, Bange HW. 2013. A new method for continuous measurements of oceanic and atmospheric N_2O, CO and CO_2: performance of off-axis integrated cavity output spectroscopy (OA-ICOS) coupled to non-dispersive infrared detection (NDIR). *Ocean Science* **9(6)**:1071–1087 DOI 10.5194/os-9-1071-2013.

Atkinson A, Whitehouse MJ, Priddle J, Cripps GC, Ward P, Brandon MA. 2001. South Georgia Antarctica: a productive, cold water, pelagic ecosystem. *Marine Ecology Progress Series* **216**:279–308 DOI 10.3354/meps216279.

Bange H. 2008. Gaseous nitrogen compounds (NO, N_2O, N_2, NH_3) in the ocean. *Nitrogen in the Marine Environment* **2**:199–261.

Bange H, Rapsomanikis S, Andreae M. 1996. Nitrous oxide in coastal waters. *Global Biogeochemical Cycles* **10(1)**:197–207 DOI 10.1029/95GB03834.

Biddle LC, Kaiser J, Heywood KJ, Thompson AF, Jenkins A. 2015. Ocean glider observations of iceberg-enhanced biological production in the northwestern Weddell Sea. *Geophysical Research Letters* **42(2)**:459–465 DOI 10.1002/2014GL062850.

Brandon MA, Murphy EJ, Trathan PN, Bone DG. 2000. Physical oceanographic conditions to the northwest of the sub-Antarctic Island of South Georgia. *Journal of Geophysical Research: Oceans* **105(C10)**:23983–23996 DOI 10.1029/2000JC900098.

Chen L, Zhang J, Zhan L, Li Y, Sun H. 2014. Differences in nitrous oxide distribution patterns between the Bering Sea basin and Indian Sector of the Southern Ocean. *Acta Oceanologica Sinica* **33(6)**:9–19 DOI 10.1007/s13131-014-0484-8.

Ciais P, Sabine C, Bala G, Bopp L, Brovkin V, Canadell J, Chhabra A, DeFries R, Galloway J, Heimann M, Jones C, Le Quéré C, Myneni RB, Thornton S, Piao P. 2013. Carbon and other biogeochemical cycles, in climate change: the physical science basis. Contribution of working group I to the fifth assessment report of the intergovernmental panel on climate change, edited by Stocker TF, Qin D, Plattner G-K, Tignor M, Allen SK, Boschung J, Nauels A, Xia Y, Bex V, and Midgley PM. Cambridge University Press, Cambridge, United Kingdom and New York, NY, USA.

Crutzen PJ. 1970. The influence of nitrogen oxides on the atmospheric ozone content. *Quarterly Journal of the Royal Meteorological Society* **96(408)**:320–325.

Deacon GER. 1979. The Weddell gyre. *Deep-Sea Research Part A Oceanographic Research Papers* **26(9)**:981–995 DOI 10.1016/0198-0149(79)90044-X.

De Baar HJW, De Jong JTM, Bakker DCE, Löscher BM, Veth C, Bathmann U, Smetacek V. 1995. Importance of iron for plankton blooms and carbon dioxide drawdown in the Southern Ocean. *Nature* **373**:412–415 DOI 10.1038/373412a0.

Devol AH. 2008. Denitrification including Anammox. *Nitrogen in the Marine Environment* **2**:199–261.

Daims H, Lebedeva EV, Pjevac P, Han P, Herbold C, Albertsen M, Jehmlich N, Palatinszky M, Vierheilig J, Bulaev A, Kirkegaard RH. 2015. Complete nitrification by Nitrospira bacteria. *Nature* **528(7583)**:555–559 DOI 10.1038/nature16461.

Dong S, Sprintall J, Gille ST, Talley L. 2008. Southern Ocean mixed-layer depth from Argo float profiles. *Journal of Geophysical Research: Oceans* **113(C6)**:C06013.

Eakins BW, Sharman GF. 2010. Volumes of the World's Oceans from ETOPO1. Boulder: NOAA National Geophysical Data Center, Boulder. *Available at https://www.ngdc.noaa.gov/mgg/global/etopo1_ocean_volumes.html*.

El-Sayed SZ, Taguchi S. 1981. Primary production and standing crop of phytoplankton along the ice-edge in the Weddell Sea. *Deep-Sea Research Part A Oceanographic Research Papers* **28(9)**:1017–1032 DOI 10.1016/0198-0149(81)90015-7.

Farías L, Florez-Leiva L, Besoain V, Sarthou G, Fernández C. 2015. Dissolved greenhouse gases (nitrous oxide and methane) associated with the naturally iron-fertilized Kerguelen region (KEOPS 2 cruise) in the Southern Ocean. *Biogeosciences* **12(6)**:1925–1940 DOI 10.5194/bg-12-1925-2015.

Fuhrman JA, Capone DG. 1991. Possible biogeochemical consequences of ocean fertilization. *Limnology and Oceanography* **36**:1951–1959 DOI 10.4319/lo.1991.36.8.1951.

Garcia HE, Locarnini RA, Boyer TP, Antonov JI, Baranova OK, Zweng MM, Reagan JR, Johnson DR. 2013. Volume 4: dissolved inorganic nutrients (phosphate, nitrate, silicate), World Ocean Atlas 2013. In: Levitus S, Mishonov A, eds. *NOAA Atlas NESDIS 76*. Silver Spring: NOAA Printing Office, 25 pp.

Gordon AL. 1967. Structure of Antarctic waters between 20°W and 170°W. *Antarctic map folio series*, Folio 6 V C. Bushnell: American Geography Society, 10 pp.

Grefe I, Kaiser J. 2014. Equilibrator-based measurements of dissolved nitrous oxide in the surface ocean using an integrated cavity output laser absorption spectrometer. *Ocean Science* **10(3)**:501–512 DOI 10.5194/os-10-501-2014.

Hande LB, Siems ST, Manton MJ. 2012. Observed trends in wind speed over the Southern Ocean. *Geophysical Research Letters* **39(11)**.

Hartmann DL, Klein Tank AMG, Rusticucci M, Alexander LV, Brönnimann S, Charabi Y, Dentener FJ, Dlugokencky EJ, Easterling DR, Kaplan A, Soden BJ, Thorne PW, Wild M, Zhai PM. 2013. Observations: atmosphere and surface. Climate change: the physical science basis. Contribution of working group I to the fifth assessment report of the intergovernmental panel on climate change, edited by Stocker TF, Qin D, Plattner G-K, Tignor M, Allen SK, Boschung J, Nauels A, Xia Y, Bex V, and Midgley PM. Cambridge University Press.

Holeton CL, Nédélec F, Sanders R, Brown L, Moore CM, Stevens DP, Heywood KJ, Statham PJ, Lucas CH. 2005. Physiological state of phytoplankton communities in the Southwest Atlantic sector of the Southern Ocean, as measured by fast repetition rate fluorometry. *Polar Biology* **29(1)**:44–52 DOI 10.1007/s00300-005-0028-y.

Jakobsson M, Macnab R, Mayer M, Anderson R, Edwards M, Hatzky J, Schenke H-W, Johnson P. 2008. An improved bathymetric portrayal of the Arctic Ocean: implications for ocean modeling and geological, geophysical and oceanographic analyses. *Geophysical Research Letters* **35**:L07602 DOI 10.1029/2008GL033520.

Jin X, Gruber N. 2003. Offsetting the radiative benefit of ocean iron fertilization by enhancing N_2O emissions. *Geophysical Research Letters* **30**:2249 DOI 10.1029/2003GL018458.

Klunder MB, Laan P, De Baar HJW, Middag R, Neven I, Van Ooijen J. 2014. Dissolved Fe across the Weddell Sea and Drake Passage: impact of DFe on nutrient uptake. *Biogeosciences* **11(3)**:651–669 DOI 10.5194/bg-11-651-2014.

Kock A, Bange HW. 2015. Counting the ocean's greenhouse gas emissions. *Eos* **96(3)**:10–13 DOI 10.1029/2015EO023665.

Korb RE, Whitehouse MJ, Thorpe SE, Gordon M. 2005. Primary production across the Scotia Sea in relation to the physico-chemical environment. *Journal of Marine Systems* **57(3–4)**:231–249 DOI 10.1016/j.jmarsys.2005.04.009.

Korb RE, Whitehouse MJ, Ward P. 2004. SeaWiFS in the southern ocean: spatial and temporal variability in phytoplankton biomass around South Georgia. *Deep-Sea Research Part II: Topical Studies in Oceanography* **51(1–3)**:99–116 DOI 10.1016/j.dsr2.2003.04.002.

Kristiansen S, Syvertsen EE, Farbrot T. 1992. Nitrogen uptake in the Weddell Sea during late winter and spring. *Polar Biology* **12(2)**:245–251 DOI 10.1007/BF00238266.

Landschützer P, Gruber N, Bakker DCE, Schuster U. 2014. Recent variability in the global ocean carbon sink. *Global Biogeochemical Cycles* **28(9)**:927–949 DOI 10.1002/2014GB004853.

Law CS, Ling RD. 2001. Nitrous oxide flux and response to increased iron availability in the Antarctic Circumpolar Current. *Deep-Sea Research Part II: Topical Studies in Oceanography* **48(11)**.

Löscher CR, Kock A, Könneke M, LaRoche J, Bange HW, Schmitz RA. 2012. Production of oceanic nitrous oxide by ammonia-oxidizing archaea. *Biogeosciences* **9(7)**:2419–2429 DOI 10.5194/bg-9-2419-2012.

Lueker TJ, Walker SJ, Vollmer MK, Keeling RF, Nevison CD, Weiss RF, Garcia HE. 2003. Coastal upwelling air-sea fluxes revealed in atmospheric observations of O_2/N_2, CO_2 and N_2O. *Geophysical Research Letters* **30(6)**:1292.

Martin JH. 1990. Glacial-Interglacial CO_2 changes: the iron hypothesis. *Paleoceanography* **5(1)**:1–13 DOI 10.1029/PA005i001p00001.

McDougall TJ, Barker PM. 2011. *Getting started with TEOS-10 and the Gibbs seawater (GSW) oceanographic toolbox.* SCOR/IAPSO WG127, 28pp.

Nelson DM, Smith WO, Muench RD, Gordon LI, Sullivan CW, Husby DM. 1989. Particulate matter and nutrient distributions in the ice-edge zone of the Weddell

Sea: relationship to hydrography during late summer. *Deep-Sea Research Part A Oceanographic Research Papers* **36(2)**:191–209 DOI 10.1016/0198-0149(89)90133-7.

Nevison CD, Keeling RF, Weiss RF, Popp BN, Jin X, Fraser PJ, Porter LW, Hess PG. 2005. Southern Ocean ventilation inferred from seasonal cycles of atmospehric N_2O and O_2/N_2 at Cape Grim, Tasmania. *Tellus Series B: Chemical and Physical Meteorology* **57(3)**:218–229 DOI 10.1111/j.1600-0889.2005.00143.x.

Nevison CD, Weiss RF, Erickson DJ. 1995. Global oceanic emissions of nitrous oxide. *Journal of Geophysical Research: Oceans* **100(C8)**:15809–15820 DOI 10.1029/95JC00684.

Nightingale PD, Malin G, Law CS, Watson AJ, Liss PS, Liddicoat MI, Boutin J, Upstill-Goddard RC. 2000. *In situ* evaluation of air-sea gas exchange parameterizations using novel conservative and volatile tracers. *Global Biogeochemical Cycles* **14(1)**:373–387 DOI 10.1029/1999GB900091.

Orsi AH, Whitworth T, Nowlin WD. 1995. On the meridional extent and fronts of the Antarctic Circumpolar Current. *Deep Sea Research Part I: Oceanographic Research Papers* **45(5)**:641–673.

Ostrom NE, Russ ME, Popp B, Rust TM, Karl DM. 2000. Mechanisms of nitrous oxide production in the subtropical North Pacific based on determinations of the isotopic abundances of nitrous oxide and di-oxygen. *Chemosphere - Global Change Science* **2(3–4)**:281–290 DOI 10.1016/S1465-9972(00)00031-3.

Priddle J, Heywood RB, Theriot E. 1986. Some environmental factors influencing phytoplankton in the Southern Ocean around South Georgia. *Polar Biology* **5**:65–79.

Randall K, Scarratt M, Levasseur M, Michaud S, Xie H, Gosselin M. 2012. First measurements of nitrous oxide in Arctic sea ice. *Journal of Geophysical Research* **117(C9)**:C00G15 DOI 10.1029/2011jc007340.

Ravishankara AR, Daniel JS, Portmann RW. 2009. Nitrous oxide (N_2O): the dominant ozone-depleting substance emitted in the 21st century. *Science* **326(5949)**:123–125 DOI 10.1126/science.1176985.

Rees AP, Brown IJ, Jayakumar A, Ward BB. 2016. The inhibition of N_2O production by ocean acidification in cold temperate and polar waters. *Deep Sea Research Part II: Topical Studies in Oceanography* **127**:93–101 DOI 10.1016/j.dsr2.2015.12.006.

Rees AP, Owens NJP, Upstill-Goddard RC. 1997. Nitrous oxide in the Bellingshausen Sea and Drake Passage. *Journal of Geophysical Research: Oceans* **102.C2**:3383–3391.

Sambrotto RN, Mace BJ. 2000. Coupling of biological and physical regimes across the Antarctic Polar Front as reflected by nitrogen production and recycling. *Deep-Sea Research Part II: Topical Studies in Oceanography* **47(15–16)**:3339–3367 DOI 10.1016/S0967-0645(00)00071-0.

Santoro AE, Buchwald C, McIlvin MR, Casciotti KL. 2011. Isotopic signature of N_2O produced by marine ammonia-oxidizing archaea. *Science* **333(6047)**:1282–1285 DOI 10.1126/science.1208239.

Sañudo Wilhelmy SA, Olsen KA, Scelfo JM, Foster TD, Flegal AR. 2002. Trace metal distributions off the antarctic peninsula in the weddell sea. *Marine Chemistry* **77(2–3)**:157–170 DOI 10.1016/S0304-4203(01)00084-6.

Smith KL, Robison BH, Helly JJ, Kaufmann RS, Ruhl HA, Shaw TJ, Twining BS, Vernet M. 2007. Free-drifting icebergs: hot spots of chemical and biological enrichment in the Weddell Sea. *Science* **317(5837)**:478–482 DOI 10.1126/science.1142834.

Smith Jr WO, Nelson DM. 1990. Phytoplankton growth and new production in the Weddell Sea marginal ice zone in the austral spring and autumn. *Limnology and Oceanography* **35(4)**:809–821 DOI 10.4319/lo.1990.35.4.0809.

Thompson AF, Heywood KJ, Thorpe SE, Renner AHH, Trasviña A. 2009. Surface circulation at the tip of the Antarctic Peninsula from drifters. *Journal of Physical Oceanography* **39(1)**:3–26 DOI 10.1175/2008JPO3995.1.

Thompson AF, Youngs MK. 2013. Surface exchange between the Weddell and Scotia Seas. *Geophysical Reserach Letters* **40**:5920–5925 DOI 10.1002/2013GL058114.

Trenberth KE, Large WG, Olson JG. 1990. The mean annual cycle in global ocean wind stress. *Journal of Physical Oceanography* **20.11**:1742–1760.

Van Kessel MA, Speth DR, Albertsen M, Nielsen PH, Den Camp HJO, Kartal B, Jetten MS, Lücker S. 2015. Complete nitrification by a single microorganism. *Nature* **528(7583)**:555–559 DOI 10.1038/nature16459.

Wadley MR, Jickells TD, Heywood KJ. 2014. The role of iron sources and transport for Southern Ocean productivity. *Deep Sea Research Part I: Oceanographic Research Papers* **87**:82–94 DOI 10.1016/j.dsr.2014.02.003.

Wallace DWR. 1995. Monitoring global ocean inventories. Inventories (Ocean Observing System Development. Panel (OOSDP)) Background Report 5. College Station: Texas A&M.

Walter S, Peeken I, Lochte K, Webb A, Bange HW. 2005. Nitrous oxide measurements during EIFEX, the European iron fertilization experiment in the subpolar South Atlantic Ocean. *Geophysical Research Letters* **32**:L23613 DOI 10.1029/2005GL024619.

Wanninkhof R. 2014. Relationship between wind speed and gas exchange over the ocean revisited. *Limnology and Oceanography: Methods* **12**:351–362.

Ward BB. 2008. Nitrification in marine systems. *Nitrogen in the Marine Environment* **2**:199–261.

Weiss RF, Price BA. 1980. Nitrous oxide solubility in water and seawater. *Marine Chemistry* **8.4**:347–359.

Weiss RF, Woy FA, Van Salameh PK, Sepanski RJ. 1992. Surface water and atmospheric carbon dioxide and nitrous oxide observations by shipboard automated gas chromatography: results from expeditions between 1977 and 1990. In: *Scripps Institution of Oceanography Reference 92-11: ORNL/CDIAC-59, NDP-044.* La Jolla: Scripps Institution of Oceanography DOI 10.2172/6726159.

Whitehouse MJ, Priddle J, Brandon MA, Swanson C. 1999. A comparison of chlorophyll/nutrient dynamics at two survey sites near South Georgia, and the potential role of planktonic nitrogen recycled by land-based predators. *Limnology and Oceanography* **44(6)**:1498–1508 DOI 10.4319/lo.1999.44.6.1498.

Whitworth T, Nowlin WD. 1987. Water masses and currents of the Southern Ocean at the Greenwich Meridian. *Journal of Geophysical Research: Oceans* **92(C6)**:6462–6476 DOI 10.1029/JC092iC06p06462.

Wrage N, Velthof GL, Van Beusichem ML, Oenema O. 2001. Role of nitrifier denitrification in the production of nitrous oxide. *Soil Biology and Biochemistry* **33(12–13)**:1723–1732 DOI 10.1016/S0038-0717(01)00096-7.

Young IR, Zieger S, Babanin AV. 2011. Global trends in wind speed and wave height. *Science* **332(6028)**:451–455 DOI 10.1126/science.1197219.

Zhan L, Chen L. 2009. Distributions of N_2O and its air-sea fluxes in seawater along cruise tracks between 30°S–67°S and in Prydz Bay, Antarctica. *Journal of Geophysical Research: Oceans* **114(C3)**:C03019.

Zhan L, Chen L, Zhang J, Yan J, Li Y, Wu M, Xu S, Lin Q, Pan J, Zhao J. 2015. Austral summer N_2O sink and source characteristics and their impact factors in Prydz Bay, Antarctica. *Journal of Geophysical Research: Oceans* **120**:5836–5849 DOI 10.1002/2015JC010944.

Grefe et al. (2018), *PeerJ*, DOI 10.7717/peerj.5100

28/28